AGU PUBLICATIONS

Geophysical Research Letters

RESEARCH LETTER
10.1002/2017GL074759

Key Points:
- For the first time, the horizontal wind divergence has been used to characterize the upper part of the polar summer mesosphere
- The higher the horizontal wind divergence is, the higher the temperature is around the mesopause
- The horizontal wind divergence field is consistent with upward vertical winds and adiabatic cooling in the mesopause region

Supporting Information:
- Supporting Information S1

Correspondence to:
F. I. Laskar,
laskar@iap-kborn.de

Citation:
Laskar, F. I., Chau, J. L., St.-Maurice, J.-P., Stober, G., Hall, C. M., Tsutsumi, M., … Hoffmann, P. (2017). Experimental evidence of arctic summer mesospheric upwelling and its connection to cold summer mesopause. *Geophysical Research Letters*, *44*, 9151–9158. https://doi.org/10.1002/2017GL074759

Received 30 JUN 2017
Accepted 25 AUG 2017
Accepted article online 30 AUG 2017
Published online 22 SEP 2017
Corrected 4 DEC 2017

This article was corrected on 4 DEC 2017. See the end of the full text for details.

Experimental Evidence of Arctic Summer Mesospheric Upwelling and Its Connection to Cold Summer Mesopause

F. I. Laskar[1], J. L. Chau[1], J. P. St.-Maurice[2], G. Stober[1], C. M. Hall[3], M. Tsutsumi[4], J. Höffner[1], and P. Hoffmann[1]

[1]Leibniz Institute of Atmospheric Physics, Kühlungsborn, Germany, [2]Department of Physics and Engineering Physics, University of Saskatchewan, Saskatoon, Saskatchewan, Canada, [3]Tromsø Geophysical Observatory, UiT The Arctic University of Norway, Tromsø, Norway, [4]National Institute of Polar Research, Tokyo, Japan

Abstract Common volume mesospheric meteor detections from two radar stations separated by about 130 km were used to retrieve horizontal wind fields between 82 and 96 km altitudes at high latitudes, near 69°N. The horizontal wind divergence was estimated from the gradients of the wind fields. This determination is the first of its kind for the mesosphere. Twelve years of nearly continuous data sets reveal systematic summer signatures in the horizontal wind divergence field, namely, a minimum just below the mesopause. There are indications that the horizontal divergence near the mesopause minimum is correlated with the mesopause temperature. Also, the altitude corresponding to the mesospheric divergence minimum tends to increase over the years. We derived the vertical velocity from the horizontal wind divergence at the mesosphere, which shows upward winds peaking near the mesopause. These winds indicate that adiabatic cooling was strongest at the region of the deep temperature minimum seen in the summer mesopause.

Plain Language Summary The lowest atmospheric temperatures on Earth are found near 90 km altitude (the mesopause) during summer at polar latitudes. This fact is now well documented and is attributed to a predominance of large amplitude gravity waves carrying eastward momentum near 90 km altitude during summer season. Through a Coriolis deflection, the deposition of this momentum causes equatorward winds at high latitudes, an expansion of the air mass, adiabatic cooling, and an accompanying upward motion of the air. In particular, an experimental determination of the upwelling has been found lacking, owing to the very small vertical motions involved. In this paper, we present a new way to determine the mean vertical motion based on the observation of summer-long-averaged horizontal wind divergences obtained by meteor radar measurements observing the same field of view from two separate locations. For 12 consecutive years we have found that the horizontal divergence shows a minimum just below the altitude where the temperature reaches its minimum value. We show that this implies upward velocities of the order of 2 to 10 cm/s reaching their peak in that same region, consistent with the notion of strong adiabatic cooling as the source of the low temperatures.

1. Introduction

The energy budget of the mesosphere is governed by radiative, photochemical, and dynamical effects. The infrared radiation emitted by greenhouse gases like CO_2 or H_2O heats the troposphere through its capture of infrared radiation emitted by the surface, while at stratospheric and mesospheric levels it provides the energy loss mechanism responsible for the balance between incoming solar radiation and outgoing Earth-generated infrared radiation (Allen et al., 1979; Beig et al., 2003). The capture of solar ultraviolet radiation by ozone drives exothermic photochemical reactions, which provide the main source of heating at stratospheric altitudes. It also acts as a minor heating agent at mesospheric levels. Wave dynamical processes can increase or reduce the mesospheric temperature through heating (by dissipation or adiabatic compression) or cooling (through adiabatic expansion). The resulting mesospheric temperature depends on the season, in association with changes in the large-scale circulation. During summer the net effect of the above three

processes results in a summer mesopause at high latitudes that is markedly colder than that inferred from radiative balance, implying that the air must be cooling adiabatically through expansion (Andrews et al., 1987; Beig et al., 2003; Liu & Roble, 2004).

Previous studies have concluded that out of the various processes mentioned above, dynamical effects due to gravity waves play a leading role in the formation of the cold summer mesopause (see, e.g., Becker, 2012; Garcia & Solomon, 1985; Gumbel & Karlsson, 2011; Sato et al., 2009; Smith, 2012). During summer, the ozone heating at high latitudes starts at a lower altitude than at the equator. This plays a crucial role in the generation of oppositely directed winds at stratospheric and tropospheric heights in summer. Under such background conditions, a strong zonal asymmetry is introduced in the gravity waves spectrum, owing to the dissipation of waves moving with the mean flow. The surviving waves reach the mesosphere where through saturation or decay, they introduce zonal forcing in a westward direction in summer (and in the eastward direction in winter). By means of the Coriolis force this introduces a residual mean meridional circulation leading, via mass conservation, to mesospheric upwelling in summer and downwelling in winter, thereby creating a global-scale interhemispheric circulation. The resulting volume expansion of the summer air cools the atmosphere adiabatically, thereby turning the summer mesosphere into the coldest region of the atmosphere, often at temperatures well below the expected radiative equilibrium value (Becker, 2012; Garcia & Solomon, 1985; Sato et al., 2009).

The above studies of the mesospheric summer dynamics in relation to cooling have emphasized the existence of upwelling as a means to arrive at adiabatic cooling. However, a quantitative direct experimental demonstration of the relationship between cooling and upwelling represents a substantial challenge, since vertical velocities of the order of a few cm s^{-1} are all that is expected (e.g., Garcia, 1989). For an indirect determination, Panofsky (1946) argued early on that the vertical velocity could be retrieved if the temperature field could be characterized fully in time and space. Alternatively, he also pointed out that the vertical wind could be retrieved through a determination of the divergence in the horizontal wind field, in what he described as the kinematic method. The only mesospheric study that we are aware of that used this approach is Dowdy et al. (2001). They used single-station high-latitude radars to estimate from the steady state mass continuity equation the zonally averaged vertical wind at a latitude that stood halfway between the pole and the observing station. They obtained, in the process, sensible profiles of the vertical winds that closely resembled model calculations. However, while showing promise, this method was devoid of local divergence measurements and subject to several assumptions about the relation between the zonally averaged winds and the local observations.

We offer here a new approach to apply the kinematic method as was used by Dowdy et al. (2001) but in an innovative way and with local measurements. This new approach uses measurements from a recent development introduced by Stober and Chau (2015), in which the horizontal wind fields were obtained locally from meteor echoes at VHF frequencies. This method, called MMARIA for "Multistatic Multifrequency Agile Radar for Investigations of the Atmosphere," derives the mesospheric wind field with separate radars looking at the same volume of air from different locations/directions. Following this approach Chau et al. (2017) have obtained 12 years of horizontal and vertical gradients of the horizontal wind fields over Northern Norway through MMARIA, allowing us to utilize the radar wind fields to apply the kinematic method. From the divergence of the resulting horizontal wind fields we present below how we can get the vertical wind (by applying some constraints through the use of a proper boundary condition), and we go on to identify regions of adiabatic cooling.

We continue with the rest of this publication by introducing the data and the methodology in section 2. Section 3 shows the results that are then discussed in section 4. The summary and conclusion are presented in section 5.

2. Data and Analysis Methodology

The primary data sets used in this study are obtained from observations of sporadic meteor echoes detected using two Specular Meteor Radars (SMRs) separated by a small but nonnegligible distance. To complement this data set, satellite and ground-based mesospheric temperature measurements are also used, as described below.

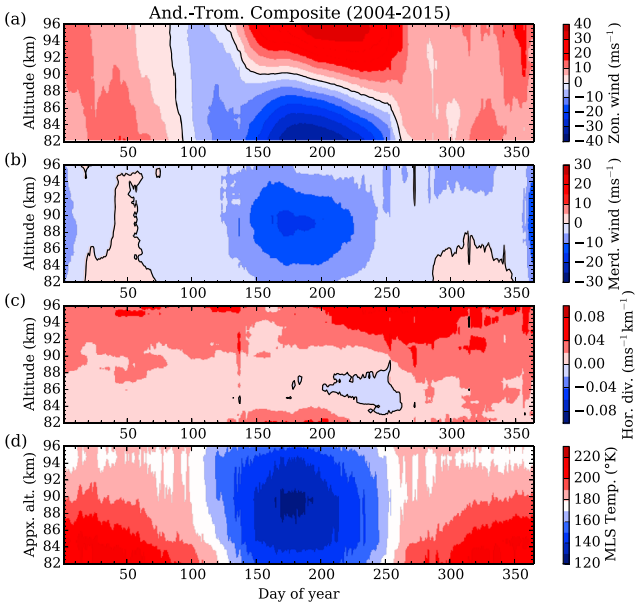

Figure 1. Composite over 2004 to 2015 of (a) zonal wind, (b) meridional wind, and (c) horizontal divergence for the common volume of observations from the two high-latitude stations near 69°N, located at Andenes (And.) and Tromsø (Trom.). (d) Composite temperatures over the stations from EOS-MLS observations of the upper mesosphere for the years 2005 to 2015 are shown.

2.1. Meteor Radar-Based Horizontal Wind Fields

The horizontal winds (zonal and meridional) and their gradients are derived using the common volume measurements from two closely separated meteor radar stations at Andenes (69°N, 16°E) and Tromsø (70°N, 19°E) in Northern Norway. The two stations are separated by approximately 130 km. As described by Stober and Chau (2015), wind field estimations have been made using a gradient wind field approach. An area with an approximate 400 km diameter is covered in the mesosphere through the observations. Not only do the data sets from the two stations provide a higher cadence, better uniformity in meteor spatial distributions than previous methods, but they also provide a common observation volume from different observing directions (Chau et al., 2017). As a result, additional spatial parameters like horizontal gradients, horizontal divergence, and relative vorticity have been derived from 12 years of observations from 2004 to 2015. The horizontal divergence is derived from the horizontal gradients $\left(\frac{\partial u}{\partial x}, \frac{\partial v}{\partial y}\right)$ as $\nabla_{\mathbf{h}} \cdot \mathbf{V}_{\mathbf{h}} = \frac{\partial u}{\partial x} + \frac{\partial v}{\partial y} - v\frac{\tan\theta}{r}$; where, u, v, and $\mathbf{V}_{\mathbf{h}}$ are for zonal, meridional, and horizontal winds, respectively, and $dx = r\cos\theta d\phi$ while $dy = r d\theta$, where θ is latitude, ϕ is longitude, and r is the distance to the center of the Earth at the observation point. The last term $\left(-v\frac{\tan\theta}{r}\right)$ is for the correction due to meridional convergence. Further details about the derivation and validation procedure of these data sets can be found in Chau et al. (2017). In that study, numerical simulations were also performed to validate the method by delineating possible instrumental or observational artifacts that could affect the derived quantities.

2.2. EOS-MLS Temperature

The Earth Observing System (EOS) Microwave Limb Sounder (MLS) is onboard a Sun synchronous polar orbiting satellite having an orbital inclination of 98°. Owing to this orbital configuration, a particular latitude sector is covered at almost fixed local times. The instrument measures remotely the atmospheric microwave emissions from its field of view in a limb viewing geometry. The kinetic temperature and other atmospheric parameters are retrieved from these thermal emission measurements, details of which can be found in Waters et al. (2006) and Schwartz et al. (2008). We use version 4.22 of the temperature data retrieval. The MLS temperatures have a typical accuracy of 3.5° K for an individual temperature profile at 0.001 hPa (about 90 km) (e.g., Schwartz et al., 2008).

3. Results

The yearly variations of the composite (daily mean over the years 2004 to 2015) zonal and meridional winds are shown in Figures 1a and 1b. The horizontal divergence derived from the wind gradients is shown in Figure 1c. A running mean of 21 days was performed on them to remove undulations associated directly with atmospheric waves. A distinct summer feature emerges from the resulting data set, namely, a minimum in horizontal divergence just below the mesopause region (about 89 km). Here note that the positive/negative values of horizontal divergence stand for regions of divergence/convergence. Related to this minimum, we can also clearly see the mesospheric temperature summer minimum in Figure 1d, which is obtained from the composite (2005–2015) MLS temperatures over 68–72°N latitudes and 0–20°E longitudes grid. The local solar times in this grid are in the ranges 3.2 ± 0.1 h and 12.1 ± 0.1 h.

The horizontal divergence data between days of year (DOY) 160 to 220 were used to investigate more closely the summer climatology. We have chosen this range of days for the following reasons: (1) Those days are away from the seasonal transition periods and (2) the mean winds, horizontal divergence, and mesospheric temperatures (shown in Figure 1) exhibit a very distinct summer pattern. In Figure 2, the resulting summer-averaged (median over DOY 160–220) divergences and their cubic fits are shown for each year from 2004 to 2015. The standard errors have been posted in the plots to provide an estimate of the uncertainty. It can be seen

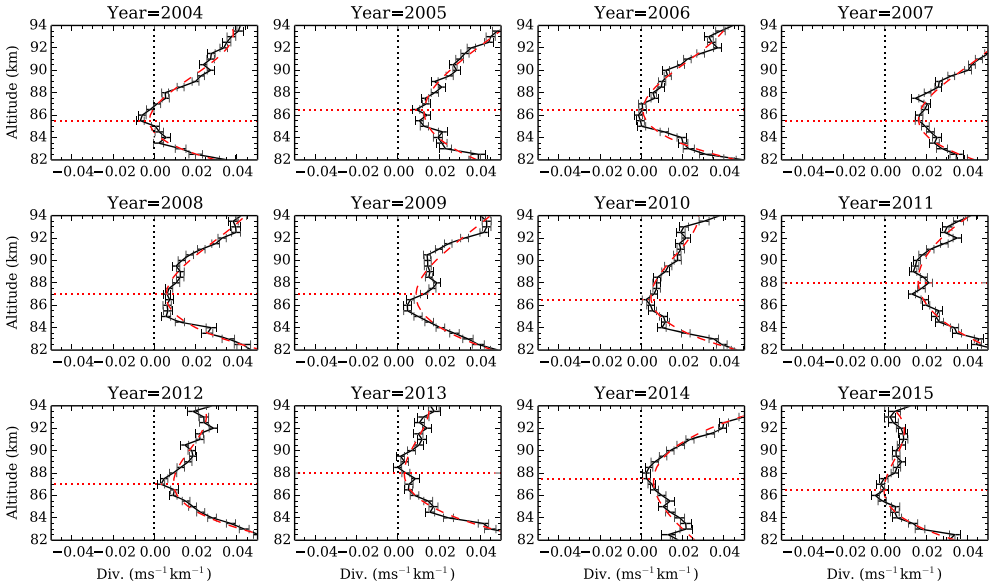

Figure 2. Full black line: year by year display of the summer (DOY 160–220) median horizontal divergence along with standard error. Dashed red line: cubic altitude fits to the horizontal divergence. A minimum in horizontal divergence is present every year just 1 or 2 km below the mesopause altitude (about 89 km) and are indicated by the dotted horizontal lines.

from Figure 2 that between 85 and 90 km, there occurs a minimum in the horizontal wind divergence . The value of the horizontal divergence corresponding to its fitted minimum near the mesopause is shown in Figure 3a.

Figure 3a also shows the EOS-MLS daily average of the temperature over 0–20°E longitude and 68–78°N latitude around the mesopause i.e., over our observation location. To enable a comparison with the minimum horizontal divergence, we have used temperatures for two levels near the mesopause, i.e., 0.001 hPa (about 90 km; T_{90}) and 0.0022 hPa (about 85 km; T_{85}). These levels are in the recommended altitude range for scientific usage (e.g., Schwartz et al., 2008). The seasonal minimum temperature (T_{85min}) obtained by fitting a second-degree polynomial to the entire summer (DOY 130 to 250) data sets are also explored. The daily data and their polynomial fit curves (to find seasonal minimum, T_{85min}) for all the years are presented in the supporting information Figure S1. Figure 3b shows the altitude of the wind divergence minimum and its linear fit for all the available years, which indicates an increasing trend in the altitude of divergence minimum over the years, at a rate of about 142 ± 55 m/yr.

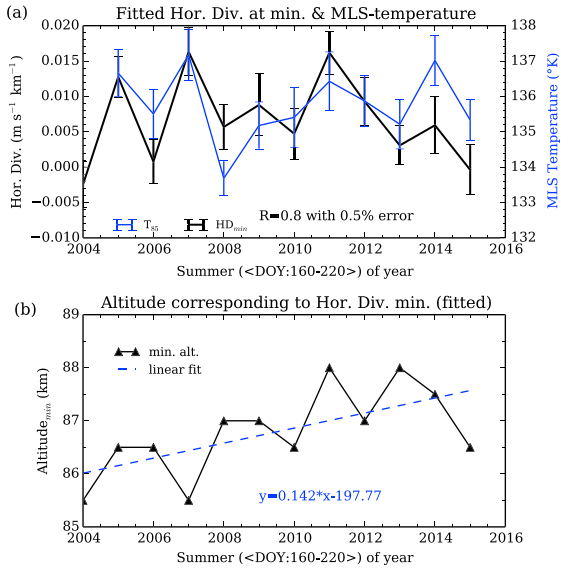

Figure 3. (a) Black line (thicker): summer (DOY 160–220) mean horizontal divergence at the fitted minimum (HD_{min}) occurring just below the mesopause. Blue line (thinner): summer mean EOS-MLS temperature at around 85 (T_{85}, 0.0022 hPa) km. A positive correlation coefficient (R) of 0.80 is observed between summer mean temperature deviations and horizontal wind divergence deviations. (b) The altitude of the divergence minimum ($Altitude_{min}$) occurring just below the mesopause are shown, which shows an increasing trend over the years.

In Figure 3 the horizontal wind divergence minimum is compared with the T_{85} only, while in the supporting information (Figure S2), comparisons are also made with T_{90} and T_{85min}. These variations show that the horizontal divergence minimum values are directly related to the temperatures around the mesopause. The Pearson correlation coefficients between detrended (deviation from next value) divergence minimum and detrended temperature are approximately equal to 0.80, 0.84, and 0.51 with respective p values around 0.005, 0.003, and 0.137 for T_{85}, T_{85min}, and T_{90}, respectively. The p values give percentage errors; e.g., there may be a 0.5% probability that the correlation between detrended divergence minimum and detrended temperature has come out of random noise. It may be noted that the above correlations vary with various factors, such as the day range being selected,

the altitude level of temperature, and the longitude and latitude range being selected. But for all reasonable ranges of the above parameters, the correlation coefficient has been found to be positive and higher than 0.4. This offers additional evidence for a connection, through the magnitudes involved, between the mesospheric minimum value in the horizontal wind divergence and the temperature near the mesopause.

4. Discussion

4.1. Inferring Adiabatic Cooling Altitude Regions From the Horizontal Divergence

Having empirically determined a relationship in the summer mesopause between the horizontal divergence and the cold temperatures in the same region, we can query the origin of this connection based on rough theoretical arguments. We start by assuming (1) that the atmosphere is anelastic for the time scale of interest ($\partial\rho/\partial t \sim \partial\rho/\partial x \sim \partial\rho/\partial y \sim 0$), and (2) that the atmosphere is in hydrostatic equilibrium.

The hydrostatic balance in a nonisothermal situation implies under the ideal gas law that we must have

$$\frac{1}{\rho}\frac{\partial \rho}{\partial z} = -\left(\frac{g}{R_s T} + \frac{1}{T}\frac{\partial T}{\partial z}\right) = -\frac{1}{H} \tag{1}$$

where, ρ, g, R_s, T, and H are the mass density, acceleration due to gravity, specific gas constant, temperature, and density scale height, respectively.

The three-dimensional mass continuity equation under the assumption of incompressibility (or anelastic conditions) then becomes

$$-\frac{w}{\rho}\frac{\partial \rho}{\partial z} = \frac{w}{H} = \boldsymbol{\nabla}_{\mathbf{h}} \cdot \mathbf{V}_{\mathbf{h}} + \frac{\partial w}{\partial z} \tag{2}$$

Since the temperature field and the horizontal divergence are retrieved from the observations, we can determine the vertical velocity from an integration of (2), which gives

$$w(z) = e^{I(z,z_i)}\left[w_i - \int_{z_i}^{z} e^{-I(z',z_i)} \boldsymbol{\nabla}_{\mathbf{h}} \cdot \mathbf{V}_{\mathbf{h}}(z')\mathrm{d}z'\right] \tag{3}$$

where $I(z, z_i) = \int_{z_i}^{z} \frac{1}{H(z'')}\mathrm{d}z''$.

An important point for the energy balance is that if we find from the calculations that the vertical velocity w is not equal to zero, then, from (2), we have to conclude that the three-dimensional wind field has a net divergence. This means that the atmosphere will be cooling off adiabatically if $w > 0$ and be heated adiabatically if $w < 0$ (Garcia, 1989), since the energy equation states that the change in the temperature (i.e., in the internal energy) due to adiabatic processes is given by $-p\nabla \cdot \mathbf{V} = -pw/H$, where $\mathbf{V}$ is the three-dimensional velocity. In a steady state situation, the cooling rate (associated with $w > 0$) would have to be balanced, for example, by a $-\mathbf{V} \cdot \nabla T$ term around the temperature minimum region. Notice that this kind of analysis does not ask whether there is a horizontal divergence in the flow nor does it describe the energy balance with any precision. These important questions have to be dealt either with the use of numerical models or with a detailed description of the temperature field in space. It remains, nonetheless, that for the summer mesopause, adiabatic cooling has to be present, implying that the air has to be moving upward in the region where the temperature is the coldest, irrespective of the details of the energy balance (which would only control the magnitude of the upward wind).

Having pointed out the significance of the sign of w, we now return to the question of the assessment of its value. A direct experimental determination of the vertical velocity is rare because its magnitude is often considerably smaller than the Doppler shift in the radial velocity. We therefore have to resort to the above cited "kinematic" method based on the continuity equation and hydrostatic balance. A central problem with the method is that the value inferred for w depends on the choice of a boundary value, w_i, from which all other values can be inferred. We therefore resorted to investigate how the solution described by equation (3) changes with various boundary conditions. However, it should be noted first that the equation indicates that

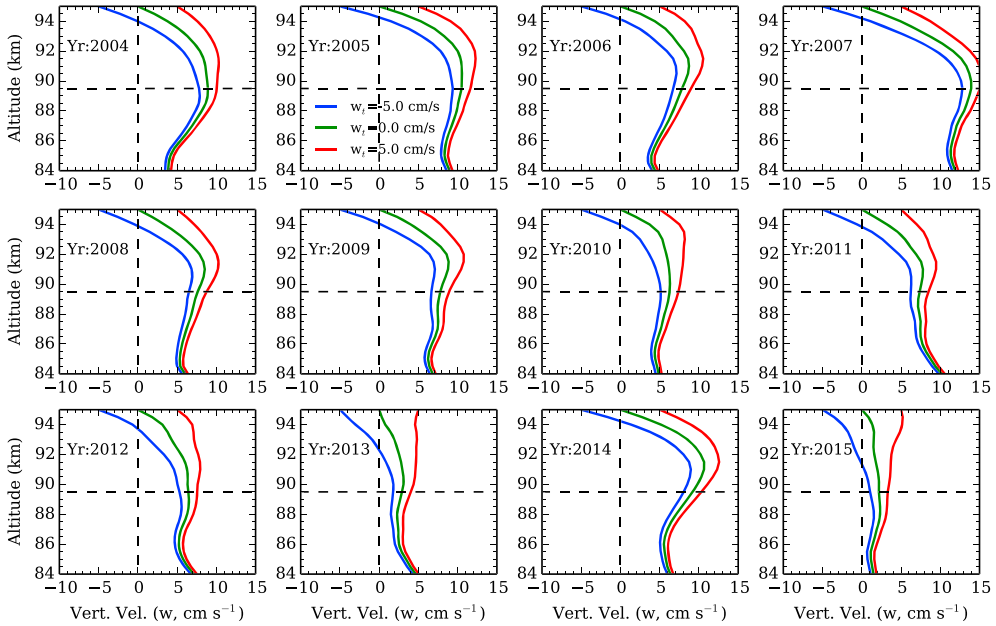

Figure 4. Vertical velocity estimated from the divergence profiles in Figure 2 with initial boundary conditions at the top (w_t) of −5, 0, and +5 cm s^{-1}. One may note that all the solutions produce a maximum w at or just 1 to 2 km above the mesopause (indicated by dotted horizontal line).

the divergence in the horizontal wind leads to vertical wind and thus to upwelling/downwelling depending on the variation of the convergence/divergence as a function of altitude. Related to this is the fact that in the absence of a horizontal wind divergence over a wide region (i.e., $\nabla_h \cdot \mathbf{V_h} \equiv 0$), the vertical wind would have to be zero, since the resulting equation would otherwise produce exponentially growing solutions as a function of altitude. Alternatively, if the horizontal wind divergence changes as a function of altitude, then it can easily be shown that w cannot be zero everywhere, namely, there has to be some upwelling or downwelling. Then the atmosphere will expand or contract and consequently cool off or heat up adiabatically owing to $\nabla \cdot \mathbf{V} = w/H \neq 0$. In short, we should expect solutions for which $w > 0$ in the regions associated with the lowest mesospheric temperatures in order to have consistency between w and the temperature fields.

In Figure 4 we show the vertical velocity profiles derived from the horizontal divergence measurements. For the calculation of the density scale height the average temperature profile of July 2015 is used (not shown here). The temperature profile came from the average Fe-lidar temperatures obtained from a nearby station at Alomar. Having no such data for the summer of other years, we used the 2015 temperature profile for the calculations of the vertical velocity for the rather different-looking horizontal divergence profiles of other years. The use of the same temperature profile assumed that the summer mesopause stays near 89 km, based on work presented by Höffner and Lübken (2007) and Lübken (1999).

In Figure 4 we have produced a number of vertical velocity profiles for a range of boundary conditions, based on equation (3) and horizontal divergence profiles shown in Figure 2. The various w boundary conditions that we considered were as follows: We used the vertical velocity at the top (95 km, $w_i = w_t$) with values equal to, −5, 0, and +5 cm s^{-1}. We note that in spite of a wide spread of top boundary conditions, the solutions become increasingly close as we move away from the top boundary. This can be understood as follows: If we were to set z to a low altitude and z_i to a top boundary much farther away from z in equation (3), the impact of w_i on the solution becomes vanishingly small. In other words, the solution with the top boundary condition $w_{top} = 0$ can be considered as being rather accurate at one scale height below the top and quite accurate at another scale height lower down. This is why all the solutions gradually get crowded in as the altitude decreases. With this in mind, it is interesting to note that, in all cases including the representative case

w_{top}=0, the vertical velocity reaches a maximum at or 1 to 2 km above the height where the temperature is a minimum (indicated by dotted horizontal line).

The numerical results of Garcia (1989) and Fritts and Luo (1995) produce vertical wind profiles near the mesopause that are very similar in shape to what we have obtained one scale height below our upper boundary, although our magnitudes are greater. To understand the implications of the numbers, we can first find the role played by vertical temperature advection by multiplying the rate of temperature change with altitude, Γ_a with the vertical velocity w_s below the temperature maximum, where $\Gamma_a \approx 2$ K km^{-1}. Equating $\partial T/\partial t$ with $w_s\Gamma_a$ gives an advection term of 10 K d^{-1}, for a typical w_s of 5 cm s^{-1}. This term brings heat to the mesopause. A term that removes cold air from the mesopause above it has a very similar magnitude. So, we can conclude that heat advection compensates for the adiabatic cooling by about 20 K d^{-1}. This however, does not tell us what the adiabatic cooling rate actually is.

To compute the effect of the adiabatic cooling rate on the temperature rate of change, we have to equate our cooling rate pw/H with the rate of change in the internal energy. Using 10 cm s^{-1} for the vertical velocity at the mesopause and c_v=717 J kg^{-1} K^{-1} gives us of the order 125 K d^{-1} at the mesopause. This is a much larger number than that computed from removal via heat advection. It means that we are either seriously overestimating the vertical velocities or that other processes are at play. Regarding the second possibility, one could invoke turbulent transport, which may well introduce the missing contributions from correlations between temperature and velocity fluctuations. However, one should also not forget that the atmospheric gravity waves that deposit their momentum near 90 km must also lose their energy in the same location. If the momentum deposition rate is to have dramatic effects, the energy deposition rate should likewise have major consequences. Needless to say, a detailed assessment of the situation is well outside the scope of the present paper. Appropriate numerical models and detailed studies of the fluctuations recorded by experiments are needed to address this important question.

4.2. Possible Connection to Changing Gravity Wave Fluxes

As just alluded to, the summer mesopause cooling has been attributed mainly to dynamical changes arising due to gravity waves and maybe also tidal forcing. It seems reasonable to assume that when the flux of gravity waves is higher at the source, the energy and momentum deposited in the mesosphere would become relatively higher. This deposited momentum would introduce higher horizontal divergence forcing and thus higher temperatures. This explains our observations of the correlated variation between near mesopause temperature and horizontal wind divergence as seen in Figure 3.

The trend for an increase in the altitude of horizontal wind divergence minimum over the years could again be associated with an evolving wave momentum deposition situation. A trend for an increase in gravity wave amplitude has been reported through observations of the gravity wave kinetic energy from both medium frequency and meteor radars through horizontal wind measurements (Hoffmann et al., 2011) at midlatitudes. Other studies have also shown a tendency for the gravity wave activity to increase in the mesosphere and lower thermosphere region (e.g., Offermann et al., 2011; Oliver et al., 2013). It has also been observed from our data that the mean zonal wind during the same period shows an increasing trend at a rate of about 69 $\pm$ 24 m/yr (figure not shown here). This may well be associated with the wave momentum deposition and associated critical level filtering, a confirmation of which requires further studies using high cadence measurements.

5. Summary and Conclusions

From 12 years of mesospheric wind field observations derived from two separate meteor radar stations, we found a minimum in the horizontal wind divergence just below the mesopause in summer. The mesopause was also very near where the vertical velocity inferred from the horizontal divergence was actually at its largest, meaning that adiabatic cooling was the greatest near the mesopause. The vertical velocities that we estimated near the mesopause, were between 2 and 15 cm s^{-1} and indicated that adiabatic cooling had to be compensated not just by vertical transport effects but also by other processes such as heating by the very waves that deposit their momentum in the same region.

Although they offered poor local time coverage, the MLS temperatures were showing a positive correlation with the horizontal divergence value at the mesopause. We likewise noticed a clear trend for the altitude

of the minimum horizontal divergence to go up over the years. We speculated that these results could be explained by considering the momentum deposition due to gravity waves, which then influence the horizontal divergence.

Our study clearly illustrates that multistation wind field measurements and their derived quantities have a great potential for improving our understanding of the MLT dynamics.

Acknowledgments
We acknowledge the support of the IAP staff for keeping the radars running. This work is partially supported by the WaTiLa project (SAW-2015-IAP-1 383). J. P. S. M. acknowledges support from the Canada Research Chair program. The wind field data of the combined systems can be obtained in HDF5 format from JLC. The authors are thankful to the EOS-Aura-MLS satellite team for the temperature data sets which are available at the Jet Propulsion Laboratory: http://mls.jpl.nasa.gov/index.php. The Fe-Lidar temperature data can be obtained from J. H. We thank Bob Vincent and the other anonymous reviewer for their creative suggestions which have improved the paper significantly.

References

Allen, D. C., Haigh, J. D., Houghton, J. T., & Simpson, C. J. S. M. (1979). Radiative cooling near the mesopause. *Nature*, *281*(5733), 660–661. https://doi.org/10.1038/281660a0

Andrews, D. G., Holton, J. R., & Leovy, C. B. (1987). *Middle Atmosphere Dynamics*. San Diego, CA: Academic Press.

Becker, E. (2012). Dynamical control of the middle atmosphere. *Space Science Reviews*, *168*(1), 283–314. https: //doi.org/10.1007/s11214-011-9841-5

Beig, G., Keckhut, P., Lowe, R. P., Roble, R. G., Mlynczak, M. G., Scheer, J., ... Fadnavis, S. (2003). Review of mesospheric temperature trends. *Reviews of Geophysics*, *41*(4), 1015. https://doi.org/10.1029/2002RG000121

Chau, J. L., Stober, G., Hall, C. M., Tsutsumi, M., Laskar, F. I., & Hoffmann, P. (2017). Polar mesospheric horizontal divergence and relative vorticity measurements using multiple specular meteor radars. *Radio Science*, *52*, 811–828. https://doi.org/10.1002/2016RS006225

Dowdy, A., Vincent, R. A., Igarashi, K., Murayama, Y., & Murphy, D. J. (2001). A comparison of mean winds and gravity wave activity in the northern and southern polar MLT. *Geophysical Research Letters*, *28*(8), 1475–1478. https://doi.org/10.1029/2000GL012576

Fritts, D. C., & Z. Luo (1995). Dynamical and radiative forcing of the summer mesopause circulation and thermal structure: 1. Mean solstice conditions. *Journal of Geophysical Research*, *100*(D2), 3119–3128. https://doi.org/10.1029/94JD02613

Garcia, R. R. (1989). Dynamics, radiation, and photochemistry in the mesosphere: Implications for the formation of noctilucent clouds. *Journal of Geophysical Research*, *94*(D12), 14,605–14,615. https://doi.org/10.1029/JD094iD12p14605

Garcia, R. R., & Solomon, S. (1985). The effect of breaking gravity waves on the dynamics and chemical composition of the mesosphere and lower thermosphere. *Journal of Geophysical Research*, *90*(D2), 3850–3868. https://doi.org/10.1029/JD090iD02p03850

Gumbel, J., & Karlsson, B. (2011). Intra- and inter-hemispheric coupling effects on the polar summer mesosphere. *Geophysical Research Letters*, *38*, L14804. https://doi.org/10.1029/2011GL047968

Hoffmann, P., Rapp, M., Singer, W., & Keuer, D. (2011). Trends of mesospheric gravity waves at northern middle latitudes during summer. *Journal of Geophysical Research*, *116*, D00P08. https://doi.org/10.1029/2011JD015717

Höffner, J., & Lübken, F.-J. (2007). Potassium lidar temperatures and densities in the mesopause region at Spitsbergen (78°.N). *Journal of Geophysical Research*, *112*, D20114. https://doi.org/10.1029/ 2007JD008612

Liu, H.-L., & Roble, R. (2004). Dynamical processes related to the atomic oxygen equinox transition. *Journal of Atmospheric and Solar-Terrestrial Physics*, *66*(6–9), 769–779. https://doi.org/10.1016/j.jastp.2004.01.024

Lübken, F.-J. (1999). Thermal structure of the Arctic summer mesosphere. *Journal of Geophysical Research*, *104*(D8), 9135–9149. https://doi.org/10.1029/1999JD900076

Offermann, D., Wintel, J., Kalicinsky, C., Knieling, P., Koppmann, R., & Steinbrecht, W. (2011). Long-term development of short-period gravity waves in middle Europe. *Journal of Geophysical Research*, *116*, D00P07. https://doi.org/10.1029/2010JD015544

Oliver, W. L., Zhang, S.-R., & Goncharenko, L. P. (2013). Is thermospheric global cooling caused by gravity waves? *Journal of Geophysical Research: Space Physics*, *118*, 3898–3908. https://doi.org/10.1002/jgra.50370

Panofsky, H. A. (1946). Methods of computing vertical motion in the atmosphere. *Journal of Meteorology*, *3*(2), 45–49. https://doi.org/10.1175/1520-0469(1946)003<0045:MOCVMI>2.0.CO;2

Sato, K., Watanabe, S., Kawatani, Y., Tomikawa, Y., Miyazaki, K., & Takahashi, M. (2009). On the origins of mesospheric gravity waves. *Geophysical Research Letters*, *36*, L19801. https://doi.org/10.1029/2009GL039908

Schwartz, M. J., Lambert, A., Manney, G. L., Read, W. G., Livesey, N. J., Froidevaux, L., ... Wu, D. L. (2008). Validation of the Aura microwave limb sounder temperature and geopotential height measurements. *Journal of Geophysical Research*, *113*, D15S11. https://doi.org/10.1029/2007JD008783

Smith, A. K. (2012). Global dynamics of the MLT. *Surveys in Geophysics*, *33*(6), 1177–1230. https://doi.org/10.1007/ s10712-012-9196-9

Stober, G., & Chau, J. L. (2015). A multistatic and multifrequency novel approach for specular meteor radars to improve wind measurements in the MLT region. *Radio Science*, *50*(5), 431–442. https://doi.org/10.1002/2014RS005591

Waters, J. W., Froidevaux, L., Harwood, R. S., Jarnot, R. F., Pickett, H. M., Read, W. G., ... Walch, M. J. (2006). The Earth Observing System Microwave Limb Sounder (EOS MLS) on the Aura satellite. *IEEE Transactions on Geoscience and Remote Sensing*, *44*(5), 1075–1092. https://doi.org/10.1109/TGRS.2006.873771

Erratum

In the originally published version of this article, there was an error in one of the conversion programs from local to geocentric coordinates. The main changes are in the obtained horizontal divergence, and the magnitudes of the resulting vertical velocity. The main content of the paper has not changed. These changes resulted in better agreement with previous studies. The resulting errors have since been corrected in the article text, figures, and supporting information. The present version may be considered the authoritative version of record.